JJMIE

Volume 5, Number 2, April 2011
ISSN 1995-6665
Pages 129- 132

Jordan Journal of Mechanical and Industrial Engineering

CFD Simulations of Drag and Separation Flow Around Ellipsoids

Yazan Taamneh*

Department of Mechanical Engineering, Tafila Technical University P. O. Box 179, 66110 Tafila, Jordan

Abstract

Computational fluid dynamics (CFD) simulations are carried out for incompressible fluid flow around ellipsoid in laminar steady axisymmetric regime ($20 \le Re \le 200$). The ratio of the major to the minor axis of the ellipsoid are ranged over *a/b* = 0.5 to 2. A commercial finite volume package FLUENT was used to analyze and visualize the nature of the flow around ellipsoids of different axis ratio. The simulation results are presented in terms of skin friction coefficient, separation angles and drag coefficient. It was found that the total drag coefficient around the ellipsoid is strongly governed by the axis ratio as well as the Reynolds number. It was observed that the Reynolds number at which the separation first occur increase with axis ratio. Separation angels and drag coefficient for special case of a sphere (*AR* = 1) was found to be in good agreement with previous experimental results and with the standard drag curve. The present study has established that commercially-available software like FLUENT can provide a reasonable good solution of complicated flow structures including flow with separation.

Keywords: CFD Simulation; Laminar Flow; Drag Coefficient ; Separation Angle.

Nomenclature

a [m] ellipsoid major diameter in the flow direction

b [m] ellipsoid minor diameter in the direction normal to the flow

AR [-] axis ratio a/b

Cd [-] total drag coefficient

Cf [-] friction drag coefficient

Cp [-] pressure drag coefficient

P [N/m2] pressure

Re [-] Reynolds number

U_∞ [m/s] free stream velocity

Vx [m/s] x-component velocity

Vr [m/s] r-component velocity

Greek Symbols

μ [Pa.s] fluid dynamic viscosity

ρ [kg/m3] fluid density

Θs [degree] separation angle

1. Introduction

The flow separation around simple and complex bluff body is one of the most important and challenging problems in fluid mechanics. The separated flow around a body is difficult to predict and results in many undesirable phenomena such as drag increase, lift loss and fluctuations in the pressure filed, etc. The accuracy of the predicted flow field depends on model equations, numerical methods and grid spacing among other factors. Experimental investigations of the steady wake behind a sphere at low Reynolds numbers have been performed by [1,2]. They found that for Reynolds numbers less than 24 the flow around the sphere is perfectly laminar, no flow separation occurs, and the flow on the downstream side of the sphere is identical to that on the upstream side. The flow past a sphere over a larger range of Reynolds numbers have been investigated experimentally by [3,4]. They found that the flow was axisymmetric and stable up to Re = 200, while in [5] found the same behavior occurring up to Re = 210. These observations are in good agreement with the calculations of [6], who investigated the linear stability of the steady axisymmetric flow past a sphere and found that the flow undergoes a regular bifurcation at a Reynolds number of about 210 and results in the development of a non-axisymmetric wake.

The use of computational fluid dynamics codes to simulate the flow around geometrically complicated shapes such as airplanes, cars and ships has become standard engineering practice in the last few years. Therefore, several authors have developed numerical techniques for calculating viscous flow, applied them to a spheroid, and compared their predictions to the experimental results previously mentioned. The numerical work has developed from solutions of the boundary layer equations with a predetermined pressure distribution [7-

* Corresponding author: ytaamneh@yahoo.com.

12]. Numerical studies of the fluid flow past different shape of spheroid particles over the Reynolds number range, 1 ≤ Re ≥ 500 at different aspect ratio are presented by [12]. They found that the effect of shape of particles on individual and total drag coefficient was small at low Reynolds number and magnifies with increasing Reynolds number. Separation points where the boundary layer leaves the surface were not clearly considered in their study. Direct numerical simulation based on spectral-type methods to simulate the flow between Re = 25 and Re =1000 were carried out by [11]. Their simulations showed that the flow past a sphere is axisymmetric up to a Reynolds number of approximately 212, and that beyond this Reynolds number the flow undergoes a transition to three-dimensionality through a regular bifurcation.

There seems to be lack of computational works on flow separation around ellipsoid in axisymmetric flow regime. Therefore, this paper aims to provide a CFD simulation study of axisymmetric viscous laminar flow around ellipsoids by using commercial finite volume package FLUENT. Another sub goal of the present study is to test whether FLUENT, a commercial Computational Fluid Dynamics (CFD) software package, is capable of providing the solutions for the problem under consideration.

2. Theoretical Formulation

2.1. Governing equations

The governing equation for laminar 2D steady-state incompressible in axisymmetric geometry are the continuity equation and the two equations of motion:

$$\rho\left[\frac{\partial v_x}{\partial x}+\frac{\partial v_r}{\partial r}+\frac{v_r}{r}\right]=0 \tag{1}$$

$$\rho\left[\frac{1}{r}\frac{\partial(rv_x^2)}{\partial x}+\frac{1}{r}\frac{\partial}{\partial r}(rv_xv_r)\right]=-\frac{\partial p}{\partial x}+\frac{1}{r}\frac{\partial}{\partial x}\left[r\mu\left(2\frac{\partial v_x}{\partial x}-\frac{2}{3}(\nabla.\vec{u})\right)\right]+\frac{1}{r}\frac{\partial}{\partial r}\left[r\mu(\frac{\partial v_x}{\partial r}+\frac{\partial v_x}{\partial x}\right] \tag{2}$$

$$\rho\left[\frac{1}{r}\frac{\partial(rv_r^2)}{\partial r}+\frac{1}{r}\frac{\partial}{\partial x}(rv_xv_r)\right]=-\frac{\partial p}{\partial r}+\frac{1}{r}\frac{\partial}{\partial x}\left[r\mu\left(2\frac{\partial v_r}{\partial r}-\frac{2}{3}(\nabla.\vec{u})\right)\right]+\frac{1}{r}\frac{\partial}{\partial x}\left[r\mu(\frac{\partial v_r}{\partial x}+\frac{\partial v_x}{\partial x}\right]-2\mu\frac{v_r}{r^2}+\frac{2\mu}{3r}(\nabla\cdot\vec{u}) \tag{3}$$

where x is the axial coordinate, r is the radial coordinate, v_x is the axial velocity and v_r is the radial velocity, p is the static pressure, μ is the molecular viscosity, ρ is the density and $\nabla\cdot\vec{u}=\frac{\partial v_x}{\partial x}+\frac{\partial v_r}{\partial r}+\frac{v_r}{r}$ no external body force is considered in this study.

2.2. Boundary conditions

The x-coordinate denote the direction of the bulk flow and along the major axis of ellipsoid. The r-coordinate is along the minor axis of the ellipsoid. Figure 1 shows the coordinate system for the 2-D ellipsoid model.

Since a half body section rotated about an axis parallel to the free stream velocity (axisymmetric body) is considered. The bottom boundary of the domain is modeled as an axis boundary.

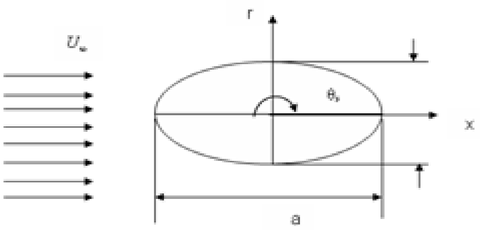

Figure 1. Schematic of the physical problem

The top and left boundaries of the domain are modeled as velocity inlet, the right boundary is modeled as an pressure out flow and the surface of the ellipsoid is modeled as a wall. Additionally, the no-slip boundary condition is assumed to hold at all fluid-solid interface, i.e. at the top surface of the ellipsoid. The boundary conditions which describing the current simulated computational domain as well as the surface boundary layer is depicted in Figure 2.

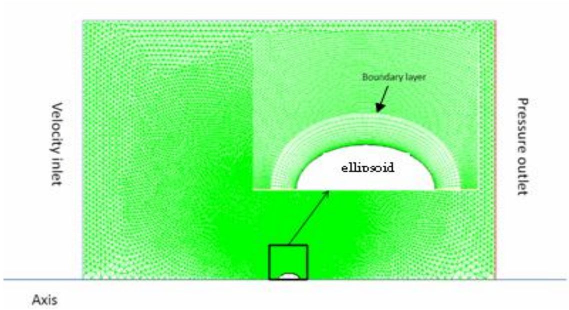

Figure 2. Solution domain and computational grid with boundary conditions and close up view of the boundary layer at *AR* = 2

3. Numerical Methods

A finite volume method is employed using a commercial software FLUENT 6.2 to solve the governing equations subject to specified boundary conditions. Since the boundary layer separation is intimately connected with the pressure and velocity distribution in the boundary layer, accurate separation point predication are dependent on accurate resolution of the boundary layer near the surface of the body. Therefore, for the purpose of grid construction, the computational domain for ellipsoid model is divided into two regions: the boundary layer region and the free stream region (see Figure 2). The boundary layers are attached to the ellipsoid and the direction of the boundary layer grid is defined such that the grids extended into the interior of the domains. More cells are constructed near the surface of the ellipsoid to compensate the high velocity gradient in the boundary layer region of the viscous flow. A commercial software GAMBIT is used for grid generation. The coupling between the pressure and velocity fields is achieved using PISO. A second order upwind schemes is used for the convection. Here in this study, following [13], we define the total drag coefficient, C_d the pressure drag coefficient, C_P the skin friction coefficient, C_f and a Reynolds number, Re as follows:

$$C_d = \frac{2D}{\rho U_\infty^2 A}, \; C_p = \frac{2(p - p_\infty)}{\rho U_\infty^2 A}, \qquad (5)$$

$$C_f = \frac{2\tau_w}{\rho U_\infty^2 A} \text{ and } \mathrm{Re} = \frac{a \cdot U_\infty \cdot \rho}{\mu}$$

where *D*, is the sum of the local skin friction and pressure drag, p_∞ is the pressure of the stream, *A* is appropriate reference area and U_∞ is free stream velocity. The grid independence is achieved by comparing the results of the different grid cell size. It was found that 75000 cells is satisfactory, and any increase beyond this size would lead to an insignificant change in the resulting solution.

4. Results and Discussion

Simulation results for axisymmetric laminar flow around sphere (*AR =1*) are compared to experimental data to verify the validity of the CFD simulation solution. Figure 3 shows the total drag coefficient as a function of Reynolds number for special case of a sphere (AR = 1). As can be seen from Figure 3, there is an excellent agreement in the Reynolds number dependence of C_d between CFD simulations in this study and the experimental measured dependence by [7].

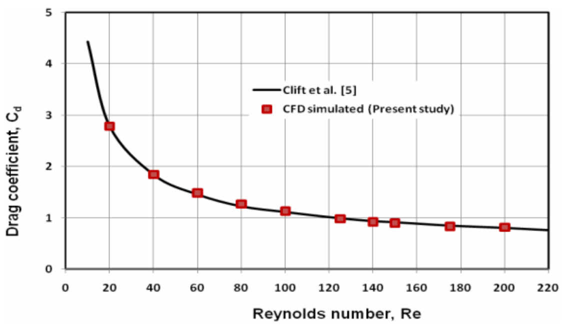

Figure 3. Comparison of computed drag coefficient with the experimental correlation of Clift et al. [5] for sphere (*AR = 1*).

The effects of Reynolds number on the total drag coefficient for ellipsoids of different axis ratio are shown in Figure 4.

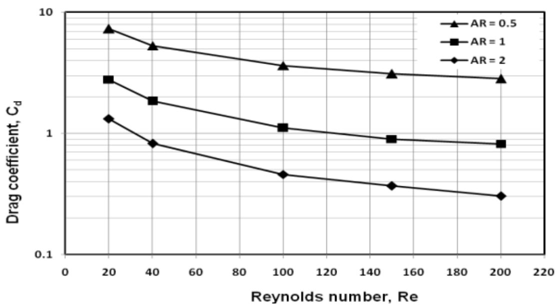

Figure 4.Variation of the total drag as a function of Reynolds number for various axis ratio.

It is clear that C_d values gradually decrease with increase in Reynolds number for all axis ratio. It can be seen that the ellipsoid of axis ratio *AR* = 2 exhibit the lowest drag coefficient due to the ellipsoid geometry. The simulated values of skin friction coefficient over the ellipsoid of different axis ratio at various Reynolds number is shown in Figure 5 (a-c).

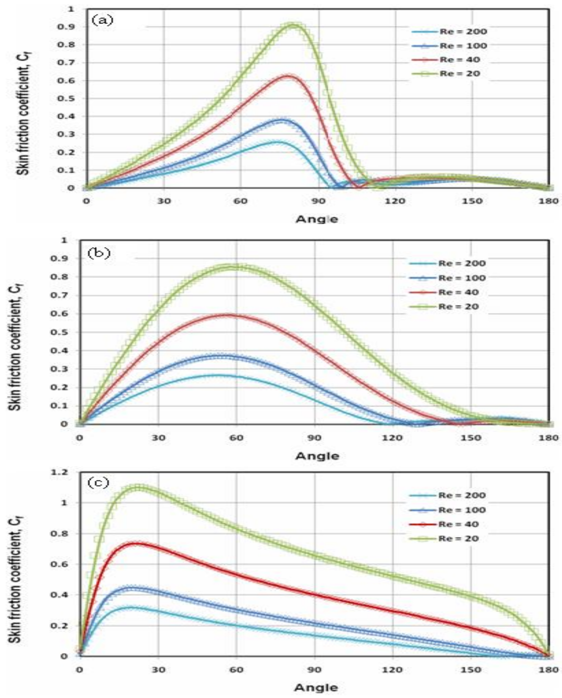

Figure 5. Skin friction coefficient on the surface of ellipsoid at different Reynolds numbers for (a) AR = 0.5, (b) AR = 1, (c) AR = 2.

It can be observed that the skin friction coefficient around the ellipsoid decreases by increasing the Reynolds number regardless of the value of axis ratio. This is due to the increase of the convection stream flow. The distribution of the skin friction coefficient identify the points where the flow leaves the surface i.e. $C_f \approx 0$. Since the point of separation itself is determined by the condition that the velocity gradient normal to the wall vanish ($\partial v_x / \partial r = 0$). It can be noted from Figure 5 (a) that the ellipsoid of axis ratio *AR* = 0.5 has always imposed to flow separation over the range of Reynolds number 20 ≤ *Re* ≤ 200. It shows that the separation angle increases with the Reynolds number from 113.5^o at *Re* = 20 to 95.29^o at *Re* = 200 (separation angle measured from the front stagnation point). For special case of sphere *AR* = 1, as Reynolds number increase beyond *Re* = 20 the separation begin to occur Figure 5(b). For the ellipsoid of axis ratio *AR* = 2 there was no separation flow except at high Reynolds number *Re* = 200, Figure 5(c). As a result, the Reynolds number at which the separation first occur increase with axis ratio. Table 1 lists the values of the angular position of separation points for all axis ratio at various Reynolds number.

The numerical prediction of separation angle values for special case of sphere *AR* = 1 matched very close Rimon and Cheng [8]. Figure 6 (a-c) shows the velocity vectors around rear half of ellipsoid for different axis ratio at Re = 200. The separation region and vortex shedding are clearly visible near the rear half of ellipsoid. It can be seen that as the axis ratio increase the separation region tends to disappear. Figure 7 (a-c) shows the velocity vectors around the rear half of ellipsoid of axis ratio *AR = 0.5* at various Reynolds number. It can be observed that as the Reynolds number increase the separation ring moves forward so that the attached recirculating wake widens and lengthens.

 © 2011 Jordan Journal of Mechanical and Industrial Engineering. All rights reserved - Volume 5, Number 2 (ISSN 1995-6665)

Table 1.Angle of separation for viscous axisymmetric laminar flow around ellipsoids.

	Separation points (in degrees, θ_s)			
Reynolds number, Re	*AR* = 0.5	*AR* = 1	*AR* = 2	*AR* = 1, [8]
20	113.4454	No separation	No separation	No separation
40	105.8824	146.7227	No separation	145.02
100	98.31932	130.084	No separation	129.37
200	95.29411	117.9832	161.8487	116.2

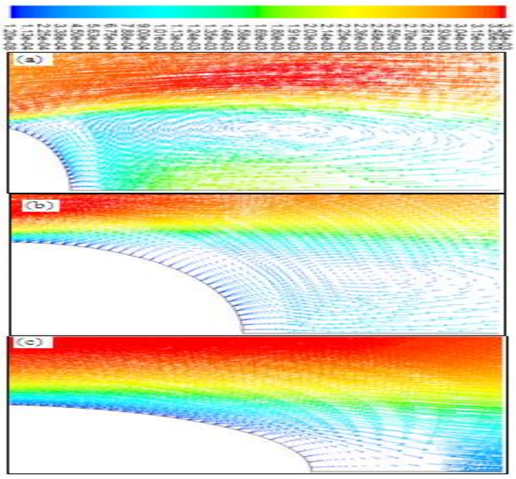

Figure 6: Velocity vectors around the rear part of the ellipsoids at Re = 200 for (a) AR = 0.5, (b) AR = 1, (c) AR = 2.

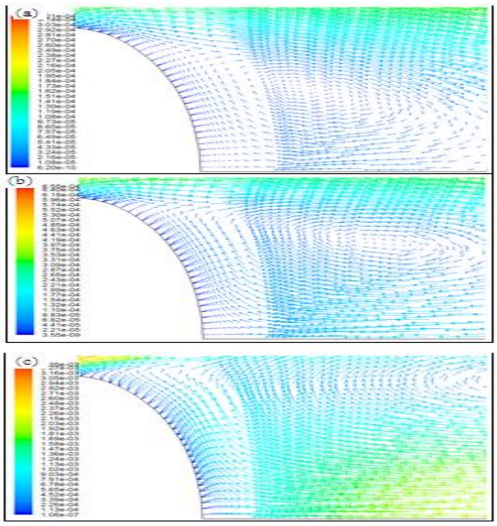

Figure 7: Velocity vectors around the rear part of the ellipsoid with AR = 0.5 for (a) Re = 20, (b) Re = 40, (c) Re = 200.

5. Conclusions

Drag and separation flow around ellipsoid in laminar steady axisymmetric region using Computational fluid dynamics (CFD) simulations are carried out. The nature of the flow around ellipsoids of different axis ratio was visualized. The dependency of the total drag coefficient on the Reynolds number and axis ratio of ellipsoids was shown. It was found that the Reynolds number at which the separation first occur increase with axis ratio i.e. for $AR \geq 2$ there may be no separation region regardless of the Reynolds number. Comparison the simulation results with the experimental data validate the commercially-available software FLUENT in providing a reasonable good solution of complicated flow structures, including flow with separation.

References

[1] S. Taneda, “Experimental Investigation of the Wake behind a Sphere at Low Reynolds Numbers”. *J. Phys. Soc. Japan*, Vol. 11, No. 10, 1956, 1104-1108.

[2] Nakamura, “Steady wake behind a sphere”, *Phys. Fluids*, Vol. 19, No. 1, 1976, 5-8.

[3] J. S. Wu, G. M. Faeth, “Sphere wakes in still surroundings at intermediate Reynolds numbers”. *AIAA J.*, Vol. 31, No. 1, 1993, 1448-1455.

[4] R. H. Margavey, R. L. Bishop,, “Transition ranges for three-dimensional wakes”. *Can. J. Phys*., Vol. 39, No. 1, 1961, 1418-1422.

[5] Clift R, Grace J. R, Weber M. E. Bubbles, Drops and Particles. New York: Academic Press. 1978.

[6] R. Natarajan, A. Acrivos, “The instability of the steady flow past spheres and disks”. J. Fluid Mech., Vol. 254, No. 3, 1993, 323-344.

[7] E. Achenbach, “Experiments on the flow past spheres at very high Reynolds numbers”. J. Fluid Mech., Vol. 54, No. 3, 1972, 565-569.

[8] Y. Rimon, S. I. Cheng, “Numerical solution of a uniform flow over a sphere at intermediate Reynolds number”. Phys. Fluid, Vol. 12, No. 1, 1969, 949.

[9] K. C. Wang, “Boundary layer over a blunt body at low incidence with circumferential flow”. J. Fluid Mech., Vol. 72, 1975, 39–65.

[10] G. S. Constantinescu, H. Pasinato, Y. Wang, J. R. Forsythe, K. D. Squires, “Numerical Investigation of Flow Past a Prolate Spheroid”. ASME J. Fluids Eng., Vol. 124, 2002, 904–910.

[11] H. W. Emmons, “The Laminar-Turbulent Transition in a Boundary Layer Part 1”. Journal of the Aeronautical Sciences, Vol. 18, No. 7, 1951, 490–498.

[12] N. N. Kumar, N. Kishore, “2-D Newtonian Flow past Ellipsoidal Particles at Moderate Reynolds Numbers”. Seventh International Conference on CFD in the Minerals and process Industries, Australia, 2009.

[13] Schlichting H. Boundary layer Theory, New York: McGraw-Hill; 1969.

[14] M. M. Karim, M. M. Rahman, M. A. Alim, “Computation of Axisymmetric Turbulent Viscous Flow Around Sphere”. Journal of Scientific Research, Vol. 1, No. 2, 2009, 209-219.

[15] C. Chang, B. Liou , R. Chern, “An analytical and Numerical study of axisymmetric flow around spheroids”. J. Fluid Mech., Vol. 234, No. 5, 1992, 219-246.